

IMAGE-BASED MOTION ANALYSIS FOR SELF-RECONFIGURABLE MOBILE ROBOT WITH INTEGRATED DOCKING

Shubhdildeep S. Sohal

Robotics and Mechatronics Lab
 Mechanical Engineering Dept.
 Virginia Tech
 Blacksburg, VA, USA
 shubh94@vt.edu

Pinhas Ben-Tzvi

Robotics and Mechatronics Lab
 Mechanical Engineering Dept.
 Virginia Tech
 Blacksburg, VA, USA
 bentzvi@vt.edu

ABSTRACT

This paper presents the design integration and experimental results of target-based autonomous locomotion of a Self-Reconfigurable Mobile Robot. Uncertainties in the sensory data can accumulate the misalignments in locomotion behavior of the robot. Such misalignments can result in a poor coupling performance resulting in the failure of the overall docked system. Therefore, it is desirable for a robot to be capable of mechanically tolerating such misalignments. As a result, a Hybrid-Wheeled mobile robot, interfaced with a 2-DOF, high misalignment tolerant coupling (GHEFT) mechanism is presented in this paper. This combined assembly is used as a source of locomotion for autonomous docking in a multi-robot assembly using Image-Based Visual Servoing (IBVS). The resulting output is then implemented in a simulated environment for the autonomous locomotion of the robot. Experimental results demonstrate the feature motion and trajectory followed under the hybrid locomotion of the robot.

Keyword: Autonomous Docking, Visual Servoing, Image processing, Target detection and tracking, Self-reconfigurable robots.

1 INTRODUCTION

Coupling is an important characteristic of modular robotic systems which makes them capable of forming long-chained rigid assemblies. In recent years, mechanical coupling has received a lot of interest due to the development of self-reconfigurable robots. It plays an important role in the stability of the overall multi-robot assembly. From lattice-based [1-2] to a mobile-based [3-4] robot, coupling joints have always been an area of interest. These properties of a robot make it versatile for various field applications. This capability is defined as Shape

Metamorphosis in the literature, namely the ability of a robot to combine with its equal counterpart to form a larger system. Each individual module equipped with such mechanisms can prove useful in environments, which are either too dangerous or inaccessible to humans, such as search and rescue applications.

The effectiveness of the coupling is defined by its ability to handle misalignment, provide a fail-safe rigid connection and being power-efficient [5-6] throughout the process. The use of pins [2], [4], hooks [7-9], magnets [1], [10], etc. classifies the versatility of such mechanism under swarm applications. These properties can vary from being Gendered [1-6] to Genderless [11], resulting in the uni-directional and bi-directional coupling. A recent survey [12] on coupling mechanisms provided a deep analysis of such mechanisms for modular reconfigurable robots. Advanced sensing and control schemes are desirable for a robot

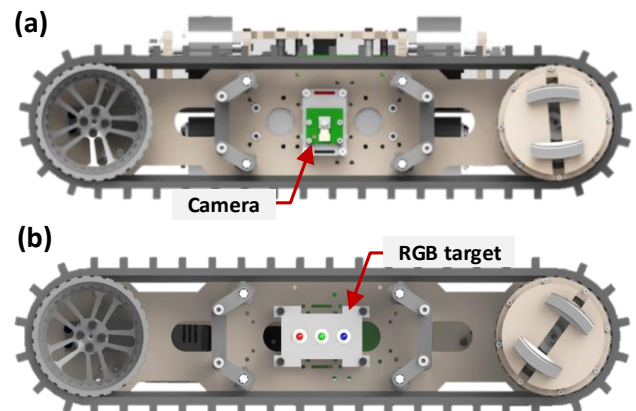


Figure 1. STORM robotic modules (a) Hybrid-Wheeled Locomotion robot (b) Manipulator robot.

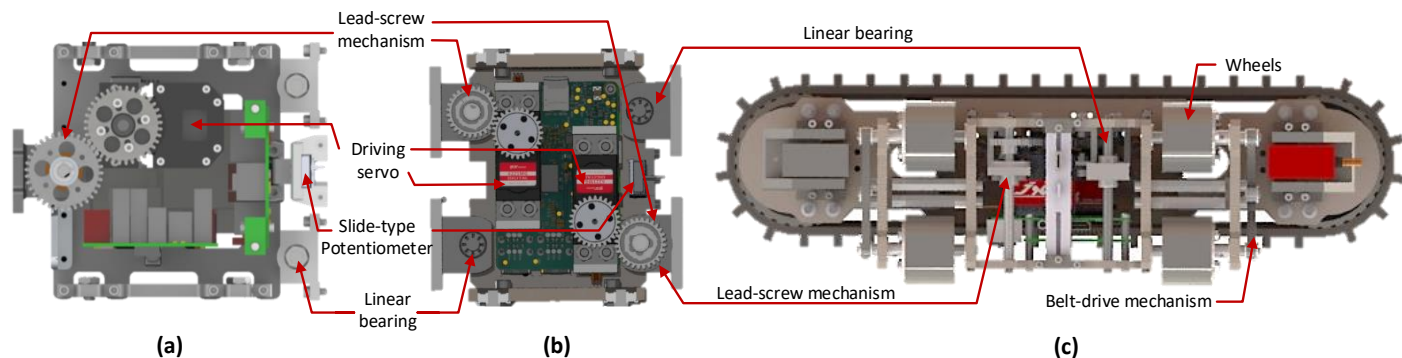


Figure 6. Vertical Translational Unit (a) single drive lead-screw mechanism, (b) new mechanism using dual drive on either side for a synchronized motion, (c) cut-section view of the locomotion robot representing the prismatic joint between the Hybrid-Wheeled assembly and the side frame of the driving mechanism.

2. *High Strength* - The mechanism can tolerate 34% higher payloads and 6% higher moments. The distribution of stress through a large surface area of the clamp makes it reliable under higher loads compared to shafts, pins or hook-type mechanisms.

3. *High Misalignment Tolerant* - Moreover, the Non-back-drivable nature of the dual spiral grooved cam makes it efficient under such instances. Since sensor and control error can get accumulated due to measurement uncertainty, a docking module should be capable of tolerating such misalignments. It can tolerate higher misalignments along with 6-DOF motion compared to the other mechanism as highlighted in this review.

The camera attached to the side frame of the locomotion robot is used as a source for analyzing the shift in the position of the target features. The operating mode of the robot (tracked/wheeled) is dependent on the position of the desired features in the Image Plane. The physical model of the robot interfaced with GHEFT has been proposed as a proof-of-concept to demonstrate autonomous docking in mobile robots. The scaled down design of the docking mechanism (reduction by 65%) is shown in Fig. 4. The Hybrid Tracked-Wheeled Multi-Directional Mobile Robot [15] is used as a primary source for analyzing the positional and angular alignment data.

The spirally grooved cam profile of the previous GHEFT design [11] (Fig. 5b) was modified to increase the number of starts from 1 to 2. Such a change helps in minimizing the offset when the clamps meet at the center in the former design. The slipping in the mechanism was removed to restrict the rotation of the mechanism to 1 full turn in either direction. This limit was implemented in the software as well as using encoder measurements. The worm-gear assembly was eliminated to incorporate a direct-drive assembly using a high torque motor connected to the coupling case of the mechanism. The motor is attached to the side frame of the robot and the coupling case is linked with a free to move/passive wheel using a ball bearing. A slide-type potentiometer is attached to the inner side of the sliding plate with a travel length of 20 mm. This potentiometer

acts as positioning feedback for the clamps. The rotary motion of the case is recorded using an encoder attached to the back end of the motor shaft controlling the rotation. The high misalignment tolerance capability of the mechanism accounts for the low 20 PPR resolution of the encoder. The sensory feedback from both devices is used for error minimization when used for positioning alignment over the TCP/IP network. The integrated mechanism can provide a maximum clamping force of 35 N and a rotational output torque of 2 Nm. According to a simulation study in SolidWorks, the maximum expected stress on the components is well below the maximum stress value of 44 MPa for the chosen material. It requires 2.74 MPa at the maximum clamping force of 35 N and 8.1 MPa at a combined load of 35 N and 1.55 Nm (rotation requirement for the robot).

Apart from these changes, the driving module of the Vertical Translational Unit (VTU) [15] was modified to house two motor-driven lead-screw mechanisms. This unit houses all the electronic components to drive the robot and to actuate the Hybrid-Wheeled assembly. The VTU is connected to a pair of a 4-wheel belt-drive mechanism to generate the lateral locomotion of the robot. The unit is connected to the main drive assembly of the robot with the help of a prismatic joint and a passive linear assembly connected to either side of the mechanism. The switch between the main drive mechanism and the Hybrid-Wheeled mechanism is done with the help of a lead screw mechanism. The motion is supported using a passive linear bearing and shaft assembly as shown in Fig. 6. The change (shown in Fig. 6) helps to eliminate the tilt while keeping the mechanism balanced from both sides as observed in the field testing of STORM. The translational feedback h_s^v of the VTU is measured using a slide-type potentiometer with a travel length of 60 mm.

The overall weight of the locomotion robot is 1.75 kg while the weight of the manipulator robot is estimated to be around 1 kg. The simulated robot has a wheelbase (L) of 310 mm, track width (W) of 250 mm, track height (H) of 92 mm and track-wheel radius (r) of 40 mm. The maximum and the minimum velocity of the tracking module is 0.345 m/sec and 0.155 m/sec, respectively.

The wheeled module operates at a maximum and minimum velocity of 0.265 m/sec and 0.22 m/sec, respectively. The VTU operates up and down at a constant velocity of 0.05 m/sec. These values have been defined based on the locomotion capability of the robot under each mode.

4 AUTONOMOUS LOCOMOTION USING IBVS

In order to demonstrate the proposed methodology of autonomous docking and the robot design, a simulation using MATLAB and V-REP is conducted. The locomotion simulation for tracking visual targets of mobile robots using the hybrid-wheeled mobility of robot is discussed in this section. The dynamic motion experimentation is done using a physics-based robotic simulator, V-REP, which was connected to MATLAB over Remote-API. The locomotion and manipulation modules of STORM were modeled in V-REP (Fig. 9) based on their CAD models designed in SolidWorks. The positioning of the robots in V-REP simulation is kept relative to the positioning of the target in the MATLAB simulation based on eye-in-hand camera configuration. The docking showed in Fig. 10 is a one-sided docking; however, both robots can be actuated in case of an intermediary obstacle or malfunction. Moreover, the validation of the proposed hypothesis is performed considering the base plane of the robots to be parallel to each other. The height difference between the modules is no more than 50 mm, taking into account the fact that the maximum VTU translation is 60 mm.

The proposed methodology includes the implementation of the Hybrid Target Tracking (HTT) algorithm [19]. HTT algorithm is a region controlled tracking algorithm which eliminates the search of the target (to be found) in the whole

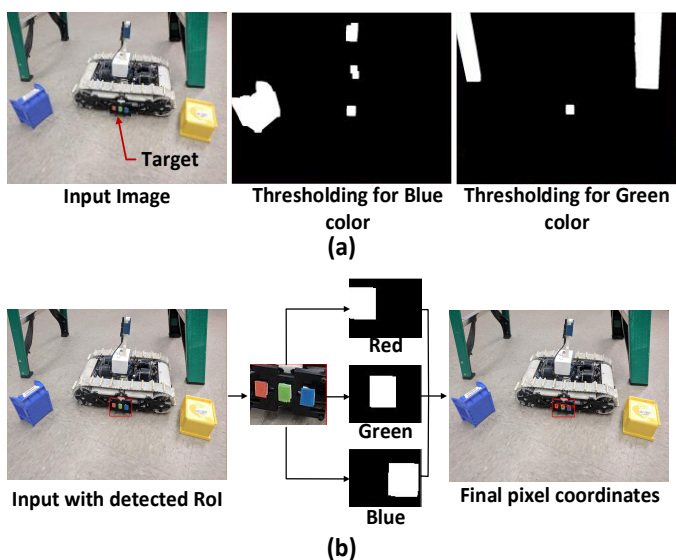


Figure 7. (a) Failure in identification of the target using color segmentation over the whole image (for green and blue) (b) Using HTT, segmenting only the Region of Interest.

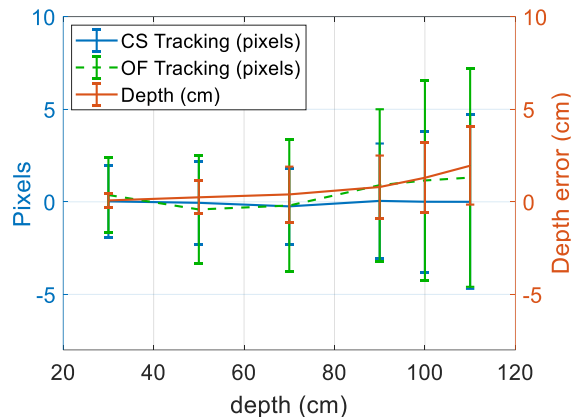


Figure 8. Mean error plot for tracking the target placed at variable distance

frame for each consecutive frames. The selected Region of Interest (RoI), based on the initial search of the target in the image frame is tracked over the consecutive frames, giving a boost to the tracking performance. The basic tracking process is shown in Fig. 7. Here, it can be seen that the use of color segmentation fails to correctly identify the actual target due to the presence of the multiple objects of the same color type. However, if the tracking process is initialized with a search of the target in the image and then the color segmentation is performed over the detected region then the algorithm is able to correctly identify and track the targets in the consecutive frames. As in this case, the RoI will include a 3-colored RGB target. This RoI will be segmented further to acquire the pixel coordinate relative to the original frame. Each of the target features is segmented separately based on the HSV color-space. These targets can be represented by $t_1^p(u_1^{roi}, v_1^{roi}), t_2^p(u_2^{roi}, v_2^{roi}), t_3^p(u_3^{roi}, v_3^{roi})$. Apart from the increase in the tracking speed, the major advantage of the HTT algorithm is to eliminate the pixelated white noise, which incurs during image segmentation due to the similarity in the pixel color values. Figure 8 represents the mean error plot, showing pixel error based on the HTT algorithm. It also shows the error for the estimated depth value with tracking varying from 30-110 cm. The deviation in the pixel value while tracking the target placed at 70cm is merely ± 4 pixels, which only decreases at the source robot moves towards the target. Since the final objective to perform the autonomous docking of the mobile robots, so, the tracking data (herein Color Segmentation (CS) data) was recorded, using Arducam 5MP camera connected to the Raspberry Pi (onboard computer of the robot). Due to the performance limitation with the hardware, a resolution value of 400x400 pixels was selected to avoid the tracking failures due to a skip or lag in the camera output. However, this error can be further minimized if a better hardware is used. In order to relate the work presented in this paper, the algorithm is used to track the motion of the features in the image

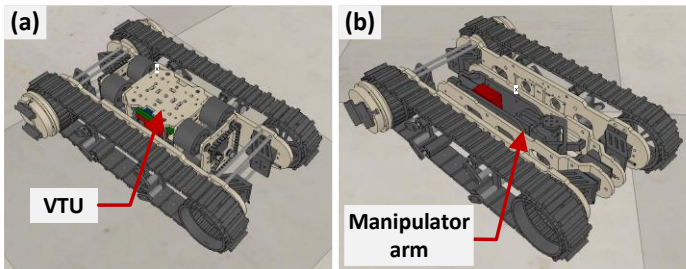


Figure 9. Geometry models designed in V-REP for simulation study, (a) Hybrid-Wheeled Locomotion module (b) Manipulator module.

plane so as to move the source robot relative to the target robot to a desired location.

However, for the purpose of the simulation results presented in this paper, it is assumed that the targets are detectable using the HTT algorithm. The markers are highlighted by Red, Green and Blue spheres as shown in Fig. 11(g). Moreover, it is also assumed that the targets are within the camera field of view. Although the docking is a two-stage process, which includes locomotion to approach [20-21] the target robot then using target tracking for autonomous docking. However, for the results presented in this paper, only the target tracking and docking stages are considered.

The parameters related to the orientation and positioning of the robots is presented in the next section considering only a single (half) side of both robots. Also, the camera is attached to only one side of the source robot in order to validate the proposed methodology.

4.1 Simulation setup

Initially, the clamps $C_s C'_s$ with height $r - h_s^v$ above the ground, of DOK-1 (Docking Mechanism 1) are positioned at extreme ends relative to its target, DOK-2 ($C_t C'_t$). The translation required for the clamping can be written as $\Delta h = h_s^v - [(h_s^c/2) + (h_t^c/2)]$, with h_s^c and h_t^c being the clamp potentiometer value of the source and the target robot. The IMU data (α – roll, β – pitch, γ – yaw) of the source (s) and the target (t) robot is defined as $\alpha_s, \alpha_t, \beta_s, \beta_t, \gamma_s$, and γ_t respectively.

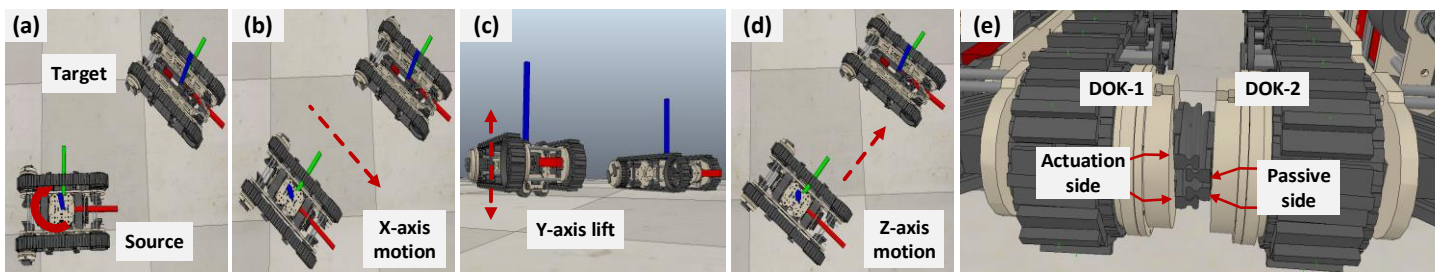


Figure 10. IBVS simulation using locomotion (source) and manipulator robot (target) shown in V-REP simulated environment, where local X, Y, Z axis are defined by bar red, blue and green, (a) Orientation alignment using TCP/IP network, (b) Translational motion along X-axis, (c) Upward lift for wheeled assembly actuation, (d) Translational motion along Z-axis, (e) Final docking for assembly reconfiguration.

The feedback from the slide-type potentiometer attached to the clamp is used to minimize the above mentioned difference. Furthermore, the orientation error between the coupling cases (θ_s, θ_t) is minimized to align the clamps of DOK-1 and DOK-2 parallel to each other. The IMU data and the potentiometer data of the VTU are further analyzed to have a configuration estimate regarding the orientation of the robot. If required, the VTU mechanism is actuated to minimize the rotation error about the Roll-Pitch-Yaw axes based on the value of h_s^v . The IMU data from both the robots ($\alpha_s, \alpha_t, \beta_s, \beta_t, \gamma_s, \gamma_t$) is then analyzed using TCP/IP network to position DOK-1 parallel to DOK-2 as shown in Fig. 10(a), 10(b). The target robot acts as a server while the locomotion robot acts as its client counterpart. This docking demonstration was done using only two robots; however the same procedure could be repeated with multiple robots to form different assemblies or configurations as shown in Fig. 2. The final error (Δe) minimization can be summarized as follows,

$$\Delta e = \min\{(\alpha_s, \beta_s, \gamma_s, h_s^c, \theta_s), (\alpha_t, \beta_t, \gamma_t, h_t^c, \theta_t)\} \quad (1)$$

The relative difference in the positions of the target and the source robot is 0.4 m, 0.05 m, 0.5m along X, Y, Z respectively, as shown in Fig. 11(g). The minor errors accumulated from the orientation alignment over TCP/IP network are further minimized under the IBVS control [22].

4.2 Experimental Result and Analysis

The simulated data is shown in Fig. 11(a) represents a curve of feature error for different modes of operation at each step. There are a total of 5 steps involved for a full motion between an initial and final position (as shown in Fig. 11(g)). At first, error along the X-axis (step-1) is minimized with reference to the center feature, followed by initial Y-estimate (step-2) as the motion along Y is subject to change with the motion along the Z-axis. This motion is followed by an initial motion along the Z-axis (step-3) in order to move the robot to the desired position before minimizing the error along the Y-axis. After the Y-axis error (step-4) is minimized, the error along the Z-axis (step-5) is minimized within an acceptable error threshold. The motion of the target features was shown in Fig. 11, highlighting the motion

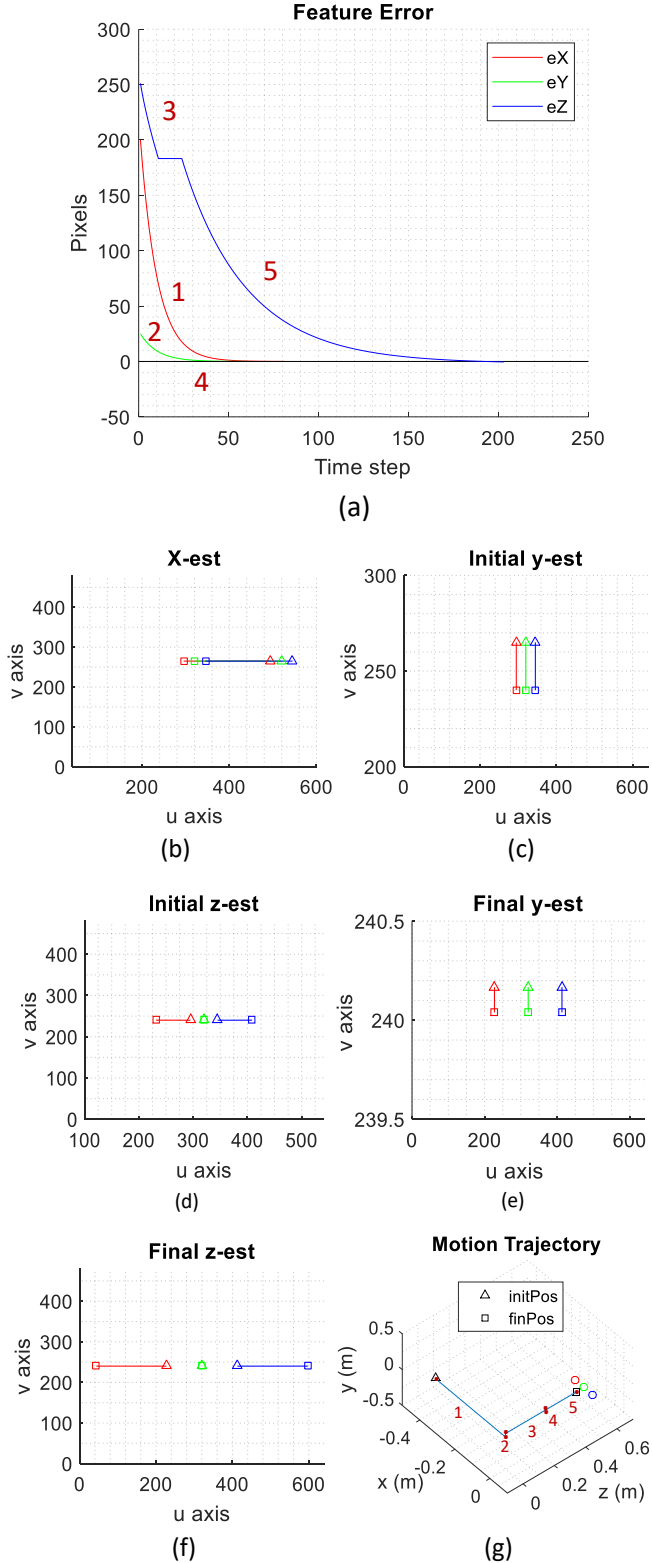


Figure 11. IBVS simulation for the autonomous docking control, (a) feature error plot, (b) feature motion along Yaw-axis, (b) X-axis, (c) Initial Y-est, (d) Initial Z-est, (e) Y-axis, (f) Z-axis, (g) Trajectory.

of the 3D point coordinate in the 2D image plane for the motion along the X-Y-Z-Yaw axes. Each of the 3D target feature spheres is represented by P_1 (Red), P_2 (Green), and P_3 (Blue).

The point projection is a mapping of a 3D coordinate to a 2D homogenous coordinate. The extrinsic camera parameters $(\Delta\alpha, \Delta\beta, \Delta\gamma)$ define the 3D point relative to the camera's 3D frame. These parameters are defined by the relative change in the IMU data value of the source and the target robot after the orientation alignment using TCP/IP network. The intrinsic parameters convert the 3D point coordinates into Image plane coordinates. The projection of the points $P_1 - P_2 - P_3$ is defined by $t_1^p - t_2^p - t_3^p$ (where $t_1^p = (u_1^p, v_1^p)$, $t_2^p = (u_2^p, v_2^p)$, $t_3^p = (u_3^p, v_3^p)$) for a desired position coordinate, $t_1^d - t_2^d - t_3^d$ (where $t_1^d = (u_1^d, v_1^d)$, $t_2^d = (u_2^d, v_2^d)$, $t_3^d = (u_3^d, v_3^d)$). The aim to minimize the error (Δe_f) between the $t_1 - t_2 - t_3$, and $t_1^d - t_2^d - t_3^d$, defined as,

$$\Delta e_f = \min\{(t_1^p, t_1^d), (t_2^p, t_2^d), (t_3^p, t_3^d)\} \quad (2)$$

Considering the motion configuration of the robot, it has 2 independent DOF in each mode and an additional DOF along Y-axis. The image interaction matrix (L) for a single feature can be written as,

$$L_i = \begin{bmatrix} -\frac{f}{\rho_u Z} & 0 & \frac{u_i}{Z} & 0 & -\frac{f^2 + \rho_u^2 u_i^2}{f} & 0 \\ 0 & -\frac{f}{\rho_v Z} & \frac{v_i}{Z} & 0 & -\frac{\rho_u f u_i v_i}{f} & 0 \end{bmatrix} \forall i = 1, 2, 3 \quad (3)$$

where f is the calibrated focal length, Z is the estimated depth value, (ρ_u, ρ_v) defines the pixel size, and (u, v) defines the pixel coordinate of the corresponding feature. Solving these parameters for all the 3 features results in an Image interaction matrix of size 6×6 . The velocity of the robot $[v_c, \omega_c]^T (= [v_x, v_y, v_z, \omega_x, \omega_y, \omega_z]^T)$ corresponds to the feature error, Δe_f , where ω_x and ω_z is 0. Based on these parameters and Eq. 3, the velocity control for the required locomotion can be written as,

$$[v_c, \omega_c]^T = \lambda ([L_1 \ L_2 \ L_3]^T)^{-1} \Delta e_f \quad (4)$$

where λ, L_1, L_2 , and L_3 represents the scalar gain, image interaction matrix of feature 1, 2, and 3 respectively. These velocity parameters (Eq. 4) are used as the velocity inputs of the source robot.

5 CONCLUSION AND FUTURE WORK

A self-reconfigurable mobile robot with integrated docking mechanism (GHEFT) was described in this paper. Specifically, this work presented the testing of autonomous docking control in a simulated environment based on the self-reconfigurable nature of the robots. MATLAB-VREP simulation involved the use of colored features as positioning targets for the locomotion robot.

The control approach incorporated the use of an image processing method, which aided in the detection and alignment of two robotic modules. IBVS control was utilized to minimize the feature error with the help of the docking mechanism.

Future work will include the use of the proposed version of the locomotion robot as a source and the target robot for autonomous docking as shown in the previous section. The colored target attached to the side frame of the target robot will be tracked using the HTT algorithm. This tracking data will be combined with the IBVS control along with TCP/IP network control for accurate alignment of the robot in a real-world environment. Furthermore, the terrain based [21] control analysis will also be covered to validate the proposed methodology in unstructured terrain for the misalignment along X-Y-Z axes and about Roll-Pitch-Yaw axes.

6 ACKNOWLEDGMENT

The authors would like to thank all the reviewers whose valuable comments helped in enhancing the quality of this paper.

REFERENCES

- [1] Romanishin, J. W., Gilpin, K., and Rus, D., "M-blocks: Momentum-driven, magnetic modular robots", International Conference on Intelligent Robots and Systems, Tokyo, 2013, pp. 4288-4295.
- [2] Yim, M., Duff, D. G. and Roufas, K. D., "PolyBot: a modular reconfigurable robot," Proc. 2000 ICRA. Millen. Conf. IEEE Int. Conf. Robot. Autom. Symp. Proc. (Cat. No. 00CH37065), San Francisco, CA, USA, 2000, pp. 514-520 vol.1.
- [3] Zhong, M., Guo, W., Li, M., Xu, J., "Tanbot: A Mobile Self-Reconfigurable Robot Enhanced with Embedded Positioning Module", 2008 IEEE Workshop on Advanced Robotics and Its Social Impacts, Taipei, 2008, pp. 1-5.
- [4] Wang, W., Yu, W., Zhang, H., "JL-2: A Mobile Multi-Robot System with Docking and Manipulating Capabilities", International Journal of Advanced Robotic Systems, Vol. 7, Issue 1, 2010.
- [5] Moubarak, P., Ben-Tzvi, P., "A Tristate Rigid Reversible and Non-Back-Drivable Active Docking Mechanism for Modular Robotics," IEEE/ASME Transactions on Mechatronics, Vol. 19, Issue 3, pp. 840-851, June 2014.
- [6] Moubarak, P. M., and Ben-Tzvi, P., "On the Dual-Rod Slider Rocker Mechanism and its applications to Tristate Rigid Active Docking," Journal of Mechanisms and Robotics, Vol. 5, Issue 1, pp. 011010:1-10, Feb. 2013.
- [7] Groß, R., Bonani, M., Mondada, F., Dorigo, M., "Autonomous self-assembly in a swarm-bot", in IEEE Transactions on Robotics, Vol. 22, Issue. 6, pp. 1115-1130, Dec. 2006.
- [8] Qiao, G., Song, G., Zhang, J., Sun, H., Wang, W., Song, A., "Design of Transmote: A modular self-reconfigurable robot with versatile transformation capabilities", Proc. Of IEEE International Conference on Robotics and Biomimetics (ROBIO), Guangzhou, 2012, pp. 1331-1336.
- [9] Wei, H. X., Li, H. Y., Guan, Y., Li, Y. D., "A dynamics based two-stage path model for the docking navigation of a self-assembly modular robot (SAMBOT), Robotica Journal. 34 (7), pp. 1517-1528, doi:10.1017/S0263574714002422.
- [10] Shirmohammadi, B., Taylor, C., Yim, M., Sastra, J., Park, M., "Using Smart Cameras to Localize Self-Assembling Modular Robots", Proc. Of the 1st ACM/IEEE International Conference on Distributed Smart Cameras, Vienna, 2007, pp. 76-80. doi: 10.1109/ICDSC.2007.4357508.
- [11] Saab, W., Ben-Tzvi, P., "A Genderless Coupling Mechanism with 6-DOF Misalignment Capability for Modular Self-Reconfigurable Robots", Journal of Mechanisms and Robotics, Transactions of the ASME, Vol. 8, Issue 6, pp. 061014:1-9, Dec. 2016.
- [12] Saab, W., Racioppo, P., Ben-Tzvi, P., "A review if coupling mechanism design for modular reconfigurable robots", Robotica Journal, October 2018. doi:10.1017/S0263574718001157.
- [13] Ben-Tzvi, P., Goldenberg, A. A., and Zu, J. W., "Articulated hybrid mobile robot mechanism with composed mobility and manipulation and onboard wireless sensor/actuator control interfaces," Mechatronics Journal, vol. 20, no. 6, pp. 627-639, Sept. 2010.
- [14] Moubarak, P. M., Alvarez, E. J., and Ben-Tzvi, P., "Reconfiguring a Modular Robot into a Humanoid Formation: A Multi-Body Dynamic Perspective On Motion Scheduling for Modules and Their Assemblies", Proc. of 2013 IEEE Int. Conf. on Autom. Sci. and Eng., Madison, Wisconsin, Aug. 17-21, 2013.
- [15] Kumar, P., Saab, W., Ben-Tzvi, P., "Design of a Multi-Directional Hybrid-Locomotion Modular Robot with Feedforward Stability Control", Proceedings of the 2017 ASME IDETC/CIE, 41st Mechanisms & Robotics Conference, Ohio, Aug. 6-9, 2017.
- [16] Moubarak, P., P. Ben-Tzvi, "Adaptive Manipulation of a Hybrid Mechanism Mobile Robot", Proc. of the 2011 IEEE International Symposium on Robotic and Sensors Environments (ROSE 2011), Canada, pp. 113-118, Sept. 17-18 2011.
- [17] Murata, S., Kakomura, K., and Kurokawa, H., "Docking Experiments of a modular robot by visual feedback", International Conference on Intelligent Robots and Systems, Beijing, 2006, pp. 625-630.
- [18] Daudelin, J., Jing, G., Tosun, T., Yim, M., Gazit, H. K., Campbell, M., "An integrated system for perception-driven autonomy with modular robots", IEEE Science Robotics, 2018. doi: 10.1126/scirobotics.aat4983
- [19] Sohal, S. S., Saab, W., Ben-Tzvi, P., "Improved Alignment Estimation for Autonomous Docking in Mobile Robots", Proc. of the 2018 ASME IDETC/CIE, 42nd Mechanisms and Robotics Conference, Quebec City, Canada, Aug. 26-29 2018.
- [20] Sebastian, B., Ben-Tzvi, P., "Physics-Based Path Planning for Autonomous Tracked Vehicles in Challenging Terrain",

Journal of Intelligent and Robotic Systems, 2018. doi:
10.1007/s10846-018-0851-3

[21] Sebastian, B., Ben-Tzvi, P., “Active disturbance rejection control for handling slip in tracked vehicle locomotion”,

Journal of Mechanisms and Robotics, Dec. 2018.
doi:10.1115/1.4042347

[22] Corke, P., “MATLAB toolboxes: robotics and vision for students and teachers”, IEEE Robotics and Automation Magazine, vol. 14, Issue 4, pp. 16-17, 2007